9-26-2022

Short Warm-Side Wet-Bulb Temperature Distribution Tails Lead to Accelerated Increases in Extreme Threshold Exceedances Under Global Warming

Yianna Sotirios Bekris
Portland State University

Short Warm-Side Wet-Bulb Temperature Distribution Tails Lead to Accelerated Increases in Extreme Threshold Exceedances Under Global Warming

by

Yianna Sotirios Bekris

A thesis submitted in partial fulfillment of the
requirements for the degree of

Master of Science
in
Geography

Thesis Committee:
Paul Loikith, Chair
Andrew Martin
Daniel Taylor-Rodriguez

Portland State University
2022

Abstract

Humid-heat extremes threaten human health and are increasing in frequency with global warming, so elucidating factors affecting their rate of change is critical. This thesis examines the role of historical (1985-2014) wet-bulb temperature distribution tail shape on the probability of wet-bulb temperature extreme threshold exceedances under 2°Celsius global warming. Analysis of global climate models and reanalysis reveals that non-Gaussian wet-bulb temperature distribution tails are common worldwide across extensive, spatially coherent regions. More rapid increases in the number of days exceeding the historical 95th percentile are projected in locations with shorter-than-Gaussian warm-side tails. Of the two primary components of wet-bulb temperature, specific humidity and temperature, specific humidity tail shape is much more closely correlated with wet-bulb temperature tail shape and future exceedances. This suggests that humidity tail shape is more influential on the rate of future changes in wet-bulb temperature extreme exceedances than temperature tail shape. Short non-Gaussian wet-bulb temperature warm tails have notable implications for dangerous humid-heat stress in regions where current-climate wet-bulb temperature extremes approach human safety limits.

Acknowledgements

Support for this work is provided by the U.S. National Science Foundation through Grant AGS-1621554. MERRA-2 data were obtained from the Goddard Earth Sciences (GES) Data and Information Services Center (DISC) website (http://disc.sci.gsfc.nasa.gov/mdisc/) and CMIP6 were downloaded from the World Climate Research Program (WCRP) website hosted by Earth System Grid Federation (ESGF) (https://esgf-node.llnl.gov/projects/cmip6/).

I would like to express my deepest gratitude to my advisor Dr. Paul Loikith for guiding me through this process; my abilities as a researcher have greatly expanded thanks to his dedicated mentorship. I would also like to thank everyone in the Climate Science Lab. A special thanks to Dr. Arielle Catalano for her extensive software development work as well as her advice in the initial stages of this project. I would also like to thank Ilan Gonzalez-Hirshfeld and Christina Aragon for helping me learn and understand Python, and Graham Taylor for his assistance in teaching me shell scripting and CDO. Thank you to Dr. Andrew Martin and Dr. Daniel Taylor-Rodriguez for their valuable insights which have enormously improved this thesis.

I also would like to thank my former coworkers at the Olympia Forestry Sciences Laboratory for all the good times in the woods gazing at plants and their endless encouragement. Thank you especially to Dr. Janet Prevéy for believing in me and guiding me in writing my first manuscript. I would also like to thank Leslie Brodie for teaching me countless technical and statistical skills and giving me the opportunity to present at conferences even though it wasn't really in my job description. Thank you to Dr. Dryw

Jones for teaching me R and introductory ecological modeling. All of this support has been priceless in my development as a researcher.

I have unending appreciation for all my friends and family who let me babble at them about wet-bulb temperature when they made the mistake of asking me how school was going. Last but not least, a most sincere thank you to my little corner of the music scene for keeping me grounded while I was glued to a computer screen for months on end.

Table of Contents

List of Tables

List of Figures

1. Introduction

Anthropogenic global warming is exacerbating extreme heat (IPCC 2021; Perkins et al., 2012), one of the deadliest types of severe weather (Barriopedro et al., 2011; Buzan et al., 2015; Robine et al., 2008). As global warming continues, extreme heat is expected to become more frequent, intense, and widespread (Alexander et al., 2006; Mora et al., 2017), even under a relatively modest 1.5°C increase above mean global pre-industrial temperatures (Dosio et al. 2018). In addition to temperature, humidity impresses upon the human experience of heat by modulating the evaporation of sweat (Davis et al. 2016; Wheeler 1991). Extreme humid-heat events are similarly projected to increase in frequency, magnitude, and duration with global warming, potentially exposing very large swaths of the global population to heat stress (Barnston et al., 2020; Coffel et al., 2017). Concurrent high humidity can markedly increase the human health risks of extreme heat (Buzan and Huber, 2020; Sherwood and Huber, 2010), demonstrated by heatwaves that have featured a moisture component which amplified their death tolls (Barriopedro et al., 2011; Fischer and Knutti, 2013; Karl and Knight, 1997; Wehner et al., 2016; Raymond et al., 2020).

Wet-bulb temperature (T_W), representing the lowest possible temperature of an air parcel at saturation, is an effective metric for appraising humid-heat stress that was initially described in the early 1900s (Haldane, 1905). However, heat stress indices which include humidity date at least to the 18th century (MacPherson, 1962) and overall, there are about 160 indices which endeavor to describe the human body's interaction with the thermal environment (de Freitas and Grigorieva, 2015). Other widely used examples include wet-bulb globe temperature, which considers T_W, solar radiation, and wind speed

(Yaglou and Minaed, 1957), and Apparent Temperature (also referred to as Heat Index), which uses temperature and relative humidity at a specific pressure to approximate the human perception of air temperature (Steadman, 1979). There have also been attempts to define humid heatwaves, such as the Apparent Temperature Heat Wave Index (Russo et al., 2017). Of these, T_W is relatively simple due to the low number of required meteorological input variables.

Sherwood and Huber (2010) proposed that a T_W of approximate human body temperature is an unequivocal human adaptability threshold. Evaporative cooling through sweating becomes insufficient to reduce body temperature to a safe level as T_W approaches and surpasses 35°C (Sherwood and Huber, 2010). The identification of this upper adaptability limit has galvanized the study of humid-heat extremes and moist-heat stress (Buzan and Huber, 2020; Coumou and Robinson, 2013; Matthews, 2018; Pal and Eltahir, 2015; Raymond et al., 2020; Zhang et al., 2021). When the upper adaptability threshold of 35°C T_W was introduced in 2010, such extreme T_W had not yet been knowingly observed, and informed estimates based on climate models showed that this threshold would likely not be breached until approximately 7°C global warming (Sherwood and Huber, 2010). This was disputed by Raymond et al. (2020), who discovered several instances exceeding 35°C T_W in weather station data, and Matthews identified a maximum of 35.4°C T_W at the hourly resolution in the European Centre for Medium-Range Weather Forecast's reanalysis dataset ERA5 (2018). Although T_W may overestimate heat stress under cloud cover (Willet and Sherwood, 2012) and underestimate heat stress in the sun (Sherwood and Huber, 2010; Willet and Sherwood,

2012), the theoretical adaptability limit universally applies to all humans, even those most well-suited to extreme conditions (Sherwood and Huber, 2010).

The threshold of 35°C T_W is specific to a human both unclothed and unmoving, and this has been recently scrutinized as underestimating heat stress in real-world conditions (Vanos et al., 2020). There is also scant experimental physiological research that substantiates the theoretical limit of 35°C T_W, but a recent experiment found young, healthy subjects' body temperatures began to rise at 31°C T_W and sometimes as low as 26°C T_W (Vecellio et al., 2022). This is supported by observational evidence of concurrent high humidity and heat, which has been consistently identified as producing the highest levels of morbidity and mortality in comparison to high heat alone, despite not being anywhere near the theoretical adaptability limit (Fischer and Knutti, 2013; Mora, et al., 2017; Schär, 2016). Occurrences of T_W pushing human physiological limits have cascading economic and societal impacts (Dunne et al., 2013). This is of particular concern in areas with future T_W climatologies that will necessitate substantial cooling infrastructures but have impaired adaptive capacities.

Considering that climate change is already increasing the occurrence of T_W extremes that challenge the human body's thermoregulatory system (Matthews, 2018; Raymond et al., 2020), understanding their changing probability is prudent in the preemptive preparation for impending warming and climate change. Temperature by itself is documented to nonlinearly increase under global warming at varying scales and at different locations (Friedrich et al., 2016; Huybers et al., 2014; Loikith et al., 2018; Seneviratne et al., 2016), but T_W includes the added parameters of humidity and pressure, rendering the increase of T_W extremes more complex than temperature alone. Humidity

affects the partitioning of latent and sensible heat flux which impacts localized warming (Miralles et al., 2014; Skinner et al., 2018; Seneviratne et al., 2010), and paradoxically T_W may not increase in concordance with temperatures on extreme temperature days (Coffel et al., 2019). Moreover, atmospheric dynamics may temper a congruent increase of T_W with global increases in temperature, especially in the tropics (Sherwood and Huber, 2010; Zhang et al., 2021). Rastogi et al. (2020) found that for heatwaves high in Apparent Temperature, there was an increase in temperature but relative humidity stayed the same, in contrast to dry heatwaves in which relative humidity decreased. There is also evidence that sources of humidity, such as soil moisture, can influence the shape of the temperature probability density function (PDF; Berg et al., 2014). These inherent complexities confound the projection of future increases in extreme T_W.

Another complicating factor in the increase of T_W extremes is the shape of the PDFs of T_W, temperature, and humidity. Although the simplest prototype of global warming is a uniform rightward shift of a temperature distribution, most locations do not have normal distributions of their seasonal daily mean temperatures (Loikith et al., 2018; Loikith and Neelin, 2019). For example, a short non-Gaussian warm-tail can more drastically increase the probability of extreme threshold exceedances with a rightward shift (Figure 1). This is relevant in the context of heat stress, as impactful extremes are found in the warm-tails of a location's temperature PDF. Therefore, the shape of the warm-tail is valuable in determining how warming will alter the future manifestation of extreme heat (Loikith et al., 2018). The non-Gaussian nature of several meteorological variables is well-established (Garfinkel and Harnick, 2017; Linz et al., 2018; Loikith et al., 2018; Loikith and Neelin, 2019; Perrson and Sura, 2018; Ruff and Neelin, 2012), but

non-Gaussianity in wet-bulb temperature distributions has not been explored to our knowledge. If non-Gaussianity is also common for T_W distributions, the shape of the tails will have implications for the probability and magnitude of future T_W extreme threshold exceedances under global warming. Due to T_W being a heat-humidity metric, it is possible the tails of temperature and humidity PDFs are also influential. We investigate the global prevalence of T_W, temperature, and specific humidity non-Gaussian tails and their influence on future T_W exceedances above the current-climate 95th percentile extreme threshold under 2°Celsius global warming.

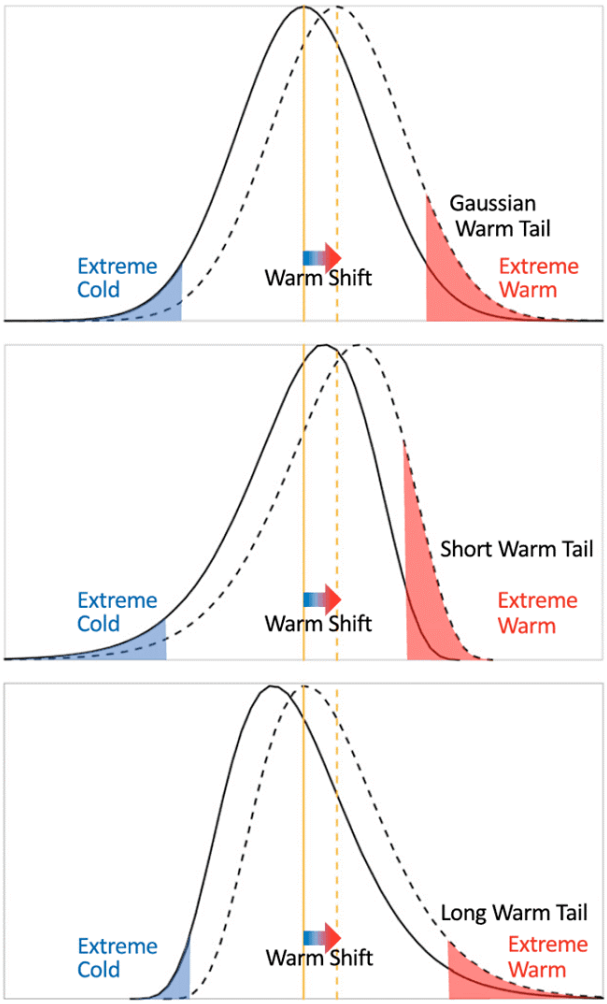

Figure 1. Shifted distributions demonstrating how tail shape can influence the manifestation of future extreme threshold exceedances. The top panel displays a Gaussian distribution, the center panel a distribution with a short non-Gaussian warm-side tail, and the bottom panel a distribution with a long non-Gaussian warm-side tail. Shaded red areas represent the warm tail, the solid line is the historical distribution, and the dashed line is the distribution under a warm shift (Loikith and Neelin, 2018).

2. Data

This analysis utilizes 31 models contributing to the sixth phase of the Coupled Model Intercomparison Project (CMIP6; Eyring et al., 2016) which were validated against reanalysis from the Modern-Era Retrospective analysis for Research and Applications, Version 2 (MERRA-2; Gelaro at al., 2015). We selected models based on the availability of the necessary meteorological variables for T_W calculation. Scenarios from CMIP6 included the pre-industrial control (piControl), historical, and the highest emission scenario ssp585. The first ensemble member of each model was used when more than one was available. Both CMIP6 models and MERRA-2 data were regridded to a 2° latitude by 2° longitude resolution using bilinear interpolation, and resampled from hourly values to a daily mean. Our analysis includes all land masses with the exception of Antarctica.

Model	Year Range	Native Resolution (latitude × longitude)
ACCESS-CM2	2023-2052	1.25° × 1.88°
ACCESS-ESM1-5	2025-2054	1.25° × 1.88°
BCC-CSM2-MR	2019-2048	1.13° × 1.13°
CanESM5	2015-2044	2.81° × 2.81°
CESM2	2023-2052	1.98° × 2.00°
CESM2-WACCM	2019-2048	0.94° × 1.25°
CMCC-CM2-SR5	2015-2044	0.94° × 1.25°
CMCC-ESM2	2019-2048	0.94° × 1.25°
CNRM-CM6-1	2024-2053	1.41° × 1.41°
CNRM-CM6-1-HR	2017-2046	0.50° × 0.50°
CNRM-ESM2-1	2032-2061	1.41° × 1.41°
EC-Earth3	2021-2050	0.70° × 0.70°
EC-Earth3-Veg	2015-2044	0.70° × 0.70°
GFDL-CM4	2026-2055	1.00° × 1.25°
GFDL-ESM4	2038-2067	1.00° × 1.25°
GISS-E2-1-G	2028-2057	2.00° × 2.50°
HadGEM3-GC31-LL	2017-2046	1.25° × 1.88°
HadGEM3-GC31-MM	2019-2048	0.56° × 0.83°
INM-CM4-8	2030-2059	1.50° × 2.00°
INM-CM5-0	2031-2060	1.50° × 2.00°
KACE-1-0-G	2015-2044	1.25° × 1.88°
KIOST-ESM	2023-2052	1.88° × 1.88°
MIROC6	2039-2068	1.41° × 1.41°
MIROC-ES2L	2032-2061	2.81° × 2.81°
MPI-ESM1-2-HR	2036-2065	0.94° × 0.94°
MPI-ESM1-2-LR	2034-2063	1.88° × 1.88°
MRI-ESM2-0	2025-2054	1.13° × 1.13
NorESM2-LM	2040-2069	1.88° × 2.50°
NorESM2-MM	2040-2069	0.94° × 1.25°
TaiESM1	2022-2051	0.94° × 1.25°
UKESM1-0-LL	2017-2046	1.25° × 1.88°

Table 1. All models used in this analysis, their 30-year ranges of simulated 2°C global warming under the ssp585 scenario, and their native spatial resolutions.

3. Methodology

T_W is calculated using a Python translation (Li, 2019) of a Matlab implementation (Kopp, 2016) of a method utilizing pseudoadiabats as detailed by Davies-Jones (2008) and employed by Buzan within the Community Land Model version 4.5 (Buzan et al., 2015). We chose this method due to its accuracy up to 40°C T_W (Davies-Jones, 2008). We computed a pre-industrial baseline global average temperature (in accordance with the IPCC-defined pre-industrial baseline period of 1850-1900; IPCC 2021) to identify the initial 30-year period in which the CMIP6 ssp585 scenario simulated 2°C global warming for each individual model (Table 1), as equilibrium climate sensitivity is highly variable within CMIP6 (Zelinka et al., 2020). We compared historical multi-model ensemble mean (MMEM) results with MERRA-2 data for 1985-2014. T_W anomaly distributions for June-July-August (JJA) and December-January-February (DJF) were created for each individual climate model and the MERRA-2 dataset at each grid cell. Gaussianity was assessed through a *shift ratio*, i.e. shifting each distribution by 0.5 standard deviations (σ) and comparing to an equivalently shifted Gaussian distribution, as follows:

1. Shift the T_W anomaly distribution by 0.5σ at each grid cell.
2. Calculate the percentage of days that exceed the pre-shifted 95th percentile, and divide by the number of exceedances expected if a Gaussian distribution is similarly shifted.

To calculate the exceedances expected from a Gaussian shift, 10,000 datasets of equal size to each grid cell dataset were randomly generated from a Gaussian distribution shifted by 0.5σ. The median of the shifts was then calculated. We chose a 0.5σ shift instead of a specified value (e.g. 1°C) to ensure the shift is proportional to the

width of the distribution. If the shift ratio is greater than one, the tail is shorter than Gaussian, and the tail is longer if the shift ratio is less than one. A shift ratio approximately equal to one is indicative of a near-Gaussian tail. This method differs from measuring skewness and can apply to more symmetrical PDFs which have short-tails on both sides of the distribution. This approach and significance test serves as a variant of the Kolmogorov–Smirnov/Lilliefors test for normality (Loikith and Neelin, 2015).

To assess the influence of historical tail shape from 1985-2014 on future extreme exceedances during the first 30-year period with mean warming of 2°C above pre-industrial climate, we calculate a *warming ratio* (as in Loikith et al., 2018) at each grid cell for each climate model using the following procedure:

1. Calculate projected exceedances of the historical 95th percentile.
2. Shift a Gaussian distribution by the simulated mean warming (in σ) and calculate the exceedances of the pre-shifted 95th percentile.
3. Divide the value from step #1 by step #2 to obtain the *warming ratio*.

A warming ratio greater than one denotes a greater increase in extreme T_W exceedances than would be expected from a Gaussian. Individual model results from these two procedures are averaged in order to produce a MMEM shift ratio and warming ratio.

We used simple linear regression to evaluate the correlation between the shift ratios of T_W, temperature, and specific humidity and the warming ratio for each individual model as well as the MMEM. The regression was conducted for summer (JJA) in the northern hemisphere and summer (DJF) in the southern hemisphere and only included grid cells on land except Antarctica. We also created an average of the

correlation coefficient *r* (Table 2). This summarizes the influence of the shift ratios on future extreme threshold exceedances as simulated by the models and as quantified by the warming ratio.

4. Results

4.1 The global prevalence of non-Gaussian tails according to CMIP6 and MERRA-2 data

As with temperature (Linz et al., 2018; Loikith et al., 2018; Loikith and Neelin, 2019; Ruff and Neelin, 2012;), results show that extensive, spatially coherent regions of non-Gaussian T_W tails are common globally (Figure 2). This is evident in CMIP6 and MERRA-2, as well as in JJA and DJF in both hemispheres. Regions with short-tails are spatially extensive across the northern and southern hemispheres in JJA and DJF. Some notable regional examples are the southeastern United States and southern Europe in JJA, and central South America and northern Australia in DJF. Long-tails are also prevalent and in agreement between the models and reanalysis, such as across the Sahara in DJF and the Arabian Peninsula in JJA, although these are not quite as widespread as short-tails.

Comparison of MERRA-2 shift ratios with CMIP6 shift ratios reveal that the models, particularly when all 31 models are averaged, realistically simulate the reanalysis non-Gaussianity of T_W. For example, the MMEM short-tails in the southeastern United States, across Europe, and throughout central America in JJA are similar in geographic extent to the short-tails in reanalysis, as are the short-tails in northern Australia and Central America in DJF. There are some locations with discrepancies between the MMEM and the reanalysis data, such as the Indian subcontinent in JJA, which is mostly long-tailed in the MMEM, but is highly heterogenous with diffuse regions of long- and short-tails embedded within close-to-Gaussian areas in MERRA-2. Because the MMEM includes 31 models, some variability and magnitude may be blunted in the process of

calculating a mean. Similarly, large areas of Gaussianity are lost in the MMEM. A broad area may be mostly Gaussian according to MERRA-2, such as across the Amazon basin and the northern Sahara desert, but the tails appear non-Gaussian in the CMIP6 data. Despite these caveats, the overall patterns of short- and long-tails are similar between the reanalysis and climate model data.

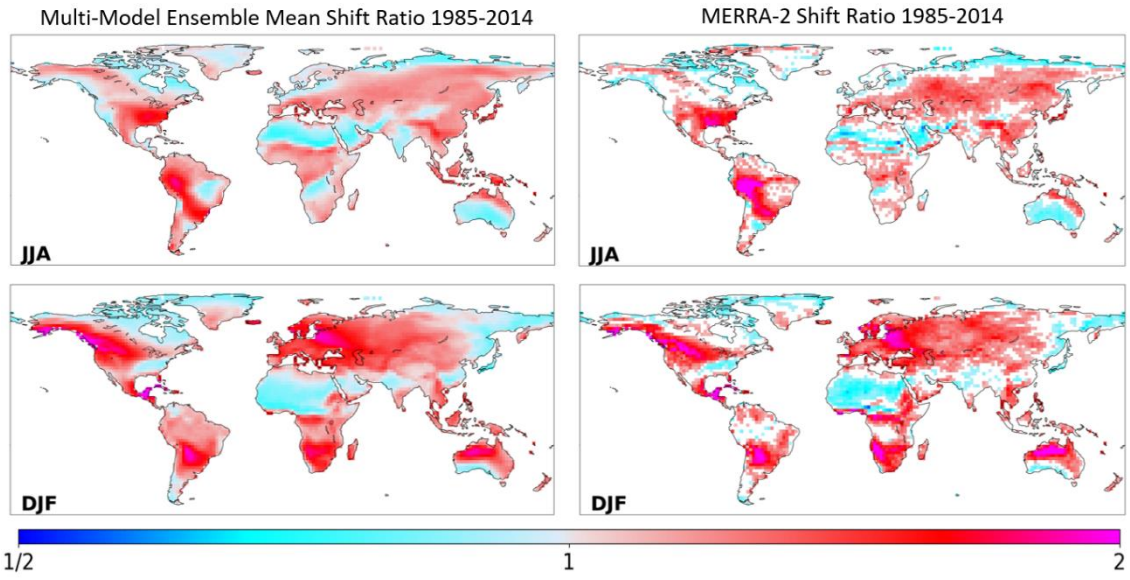

Figure 2. Shift ratio maps for MERRA-2 and the CMIP6 multi-model ensemble mean. Values larger than one (red hues) indicate a short-tail and thus a larger number of exceedances with a warm shift than if the distribution were Gaussian. Values less than one (blue hues) signify a long-tail and a lower number of exceedances than if the distribution were Gaussian. Long-tails indicate further excursions from the mean. White grid cells on land represent a warm tail that is not significantly different from a Gaussian. Models generally agreed with each other in regards to tail shape, and the MMEM shift ratios correspond with MERRA-2 shift ratios.

4.2 The warming ratio and projected extreme threshold exceedances

The shift ratio together with the warming ratio demonstrates the distinct effect that tail shape has on future extreme exceedances (Figure 3). Areas with short-tails generally coincide with regions that are projected to see a greater increase in the number of exceedances than if the distribution were Gaussian, and areas with long-tails are projected to see a smaller number of exceedances than a Gaussian. The warming ratios have more variation between models than the shift ratios; nonetheless, patterns were similar between the two metrics. Most locations with a short-tail exhibit a faster-than-Gaussian increase in extreme threshold exceedances, with some exceptions, such as the central-western and southeastern coast of Australia in JJA, and the southeastern United States in DJF. There is only subtle incongruence between the shift ratio and warming ratio, exemplified by their coincident extent across the entirety of North America in JJA, South America in DJF, Australia in DJF, Africa in DJF, and Southeast Asia in JJA.

Although areas with long-tails will not observe as expedient of an increase in the number of exceedances, the exceedances that occur can be very far from the current and future mean T_W, possibly dangerously high. Such locations in very high T_W environments may be the most at-risk of exceeding the 35°C adaptability threshold, even though the rate of increase in exceedances above the historical 95th percentile threshold will be slower than for shorter-tailed locations. Some areas with long warm-tails, such as some regions on the Indian subcontinent, already observe very extreme T_W (Im et al., 2017; van Oldenborgh et al., 2018), so this may indicate T_W that grazes or even breaches the adaptability threshold under 2°C global warming. Other long-tailed locations, such as in the Sahara, may be exposed to extreme high T_W that are so anomalous that existing

infrastructure is lacking in its ability to safely cool the population. In this sense, long-tails may assist in the identification of areas which are at risk of very rare, but very large, excursions from the mean, such as was witnessed with dry-bulb temperature in the June 2021 heatwave in the Pacific Northwest of the United States.

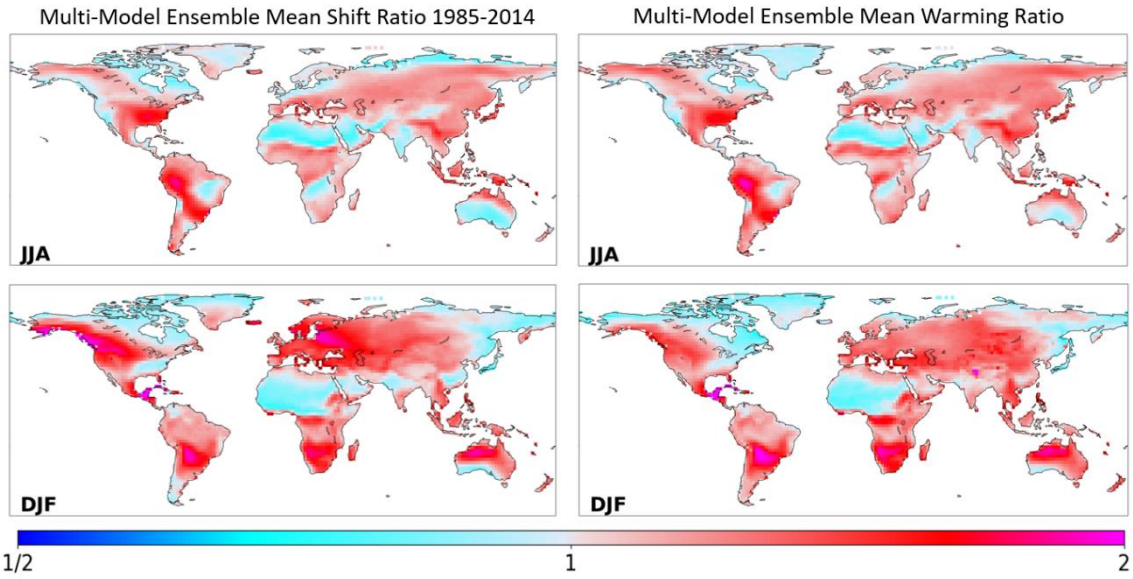

Figure 3. Shift ratio (left) and warming ratio (right) multi-model ensemble means. Values greater than one indicate a larger increase in the number of T_W extreme threshold exceedances under warming than if the underlying distribution were Gaussian.

4.3 Correlations between the T_W warming ratio and the shift ratios of specific humidity, temperature, and T_W

We ran a simple linear regression on shift ratios and the warming ratio for all individual models and averaged results of the model regression correlation coefficients, as well as the MMEM humidity, temperature, and T_W shift ratios and T_W warming ratio (Table 2). The shift ratios of specific humidity and temperature also demonstrate significant non-Gaussianity in their probability distributions, which may or may not resemble the T_W shift ratio. To investigate the correlation between the Gaussianity of specific humidity, temperature, and T_W, we conducted similar linear regression on the shift ratios of specific humidity and temperature with the shift ratio of T_W as the dependent variable. The shift ratio of specific humidity is much more closely correlated with the shift ratio of T_W (MMEM $r = 0.87$) than the shift ratio of temperature is with the shift ratio of T_W (MMEM $r = 0.28$).

To quantify the relationship between each shift ratio and T_W warming ratio, we conducted a simple linear regression with each shift ratio as the explanatory variable and the T_W warming ratio as the dependent variable. The correlation between the shift ratio and projected extreme threshold exceedances is at its strongest when utilizing the shift ratio for T_W (MMEM $r = 0.95$; Table 2), but the relative roles of temperature and specific humidity are also meaningful. The non-Gaussianity of T_W sometimes follows the pattern of temperature non-Gaussianity (Figures A1 and A2), but our analysis suggests that specific humidity has a more direct influence on T_W PDF shape than temperature. The dry-bulb temperature shift ratio is only weakly correlated with the T_W warming ratio (MMEM $r = 0.25$; Table 2), while the shift ratio for specific humidity is more closely

correlated (MMEM $r = 0.80$; Table 2)**.** There is some variability between models. CNRM-CM6-1, CNRM-CM6-1-HR, CNRM-ESM2-1, and EC-Earth3 show a weak negative correlation between the temperature shift ratio and the warming ratio, while CNRM-CM6-1 and CNRM-ESM2-1 also have a weak negative correlation between temperature shift ratio and the T_W shift ratio. Aside from these exceptions, all other models in our analysis exhibit similar patterns of correlation.

Due to the Clausius-Clapeyron relation, specific humidity is expected to scale with temperature as climates warm (Held and Soden, 2000; Santer et al., 2007; Willet et al., 2007). This relationship results in an approximate 7% increase in atmospheric moisture-holding capacity per each 1°C increase in temperature, although this can differ over the ocean and land, and there are other considerations, such as higher temperatures reducing specific humidity by increasing surface drying (Coffel et al., 2019). While a more complete understanding of the physical mechanisms that comprise the contributions from both components of T_W is beyond the scope of this research, this has important implications in the assessment and projections of humid-heat extremes. These results suggest that the presence of a short warm tail in the humidity distribution in high temperature areas may be more indicative of large increases in heat stress risk under global warming than temperature.

Model	T_W SR-T_W WR	T SR-T_W WR	Q SR-T_W WR	T SR-T_W SR	Q SR-T_W SR
ACCESS-CM2	0.88	0.21	0.76	0.29	0.84
ACCESS-ESM1-5	0.82	0.23	0.68	0.35	0.86
BCC-CSM2-MR	0.82	0.31	0.66	0.34	0.76
CanESM5	0.87	0.10	0.77	0.14	0.84
CESM2	0.76	0.14	0.79	0.37	0.83
CESM2-WACCM	0.88	0.26	0.76	0.39	0.83
CMCC-CM2-SR5	0.26	0.11	0.22	0.23	0.90
CMCC-ESM2	0.78	0.27	0.77	0.35	0.89
CNRM-CM6-1	0.80	-0.08	0.57	-0.02	0.76
CNRM-CM6-1-HR	0.85	-0.01	0.67	0.03	0.82
CNRM-ESM2-1	0.83	-0.02	0.58	-0.02	0.79
EC-Earth3	0.42	-0.18	0.31	0.13	0.80
EC-Earth3-Veg	0.84	0.12	0.74	0.25	0.76
GFDL-CM4	0.83	0.29	0.69	0.42	0.82
GFDL-ESM4	0.87	0.29	0.68	0.33	0.82
GISS-E2-1-G	0.77	0.42	0.75	0.41	0.83
HadGEM3-GC31-LL	0.82	0.28	0.69	0.35	0.79
HadGEM3-GC31-MM	0.83	0.26	0.68	0.35	0.78
INM-CM4-8	0.81	0.17	0.67	0.35	0.82
INM-CM5-0	0.80	0.14	0.66	0.31	0.84
KACE-1-0-G	0.65	0.11	0.57	0.17	0.72
KIOST-ESM	0.88	0.35	0.72	0.38	0.83
MIROC6	0.90	0.15	0.68	0.13	0.74
MIROC-ES2L	0.88	0.34	0.69	0.34	0.76
MPI-ESM1-2-HR	0.88	0.18	0.70	0.20	0.79
MPI-ESM1-2-LR	0.87	0.27	0.66	0.25	0.77
MRI-ESM2-0	0.90	0.21	0.77	0.27	0.86
NorESM2-LM	0.87	0.29	0.67	0.35	0.82
NorESM2-MM	0.89	0.38	0.68	0.48	0.78
TaiESM1	0.82	0.30	0.67	0.37	0.87
UKESM1-0-LL	0.88	0.28	0.77	0.33	0.80
Average	0.80	0.20	0.67	0.28	0.81
MMEM	**0.95**	**0.25**	**0.80**	**0.28**	**0.87**

Table 2. Linear regression coefficients for the: (first column) T_W shift ratio (SR) and the T_W warming ratio (WR); (second column) 2-meter temperature (T) SR and the T_W WR; (third column) 2-meter specific humidity (Q) SR and the T_W WR; (fourth column) temperature SR and the T_W SR; and (fifth column) the specific humidity SR and the T_W SR. All p-values are under 0.05. This regression only includes values on land for JJA in the northern hemisphere and DJF in the southern hemisphere. The "Average" row is the mean of all model r values. A visual representation of these results is available in the Appendix (Figure A5).

4.4 Example short-tailed locations

We examined four locations with short-tailed distributions: Ras Al Khaimah, United Arab Emirates; New Orleans, United States; Larkana, Pakistan, Asunción, Paraguay. A Gaussian distribution was fit to the core of the non-Gaussian PDF created from MERRA-2 anomaly data (Figure 4). We shifted the MERRA-2 T_W array by the local simulated change in warming divided by the historical σ ($\Delta T_W/\sigma_{historical}$; as in Figures A6 and A). This is a uniform shift which assumes no changes in variance, skewness, or kurtosis. Histograms from short-tailed locations as indicated by MERRA-2 data for the period of 1985-2014 are shifted by the MMEM $\Delta T_W/\sigma_{historical}$ with the simulated rise in global average temperature of 2°C since the pre-industrial era.

These cities will each have a very large percentage of days over the 1985-2014 percentile in the future. Panel (a), Ras Al Khaimah on the Persian Gulf Coast, displays a shift in extreme T_W days translating to a substantial portion of the summer months as being inhospitable to humans, with a projected 58.41% of days over the historical 95th percentile threshold of 27.33°C T_W. Panels (b-d), New Orleans, Larkana, and Asunción, also are projected to see a large rise in extreme humid-heat days every summer. Their percentage of days over their current-climate 95th percentiles (New Orleans: 26.03 °C T_W; Larkana: 25.91 °C T_W; Asunción: 25.25 °°C T_W) is projected to be 51.09%, 28.95%, and 20.33%, respectively.

In some places, especially for those with relatively low T_W variance, the recent-climate 95th percentile will be exceeded most of the time under 2°C of warming. In these locations, tail shape is not as relevant to the rate of increase because a small amount of warming will shift most of the distribution to the right of the 95th percentile. Therefore,

we have only included examples of locations with sufficiently large variance (σ greater than 1°C) for tail shape to influence future increases in extreme threshold exceedances. To illustrate this effect for cases where warming will lead to a very large number of days exceeding the historical extreme threshold, but where variance is small and the influence of warm-tail shape is dampened, we provide some examples in the Appendix (Figure A7).

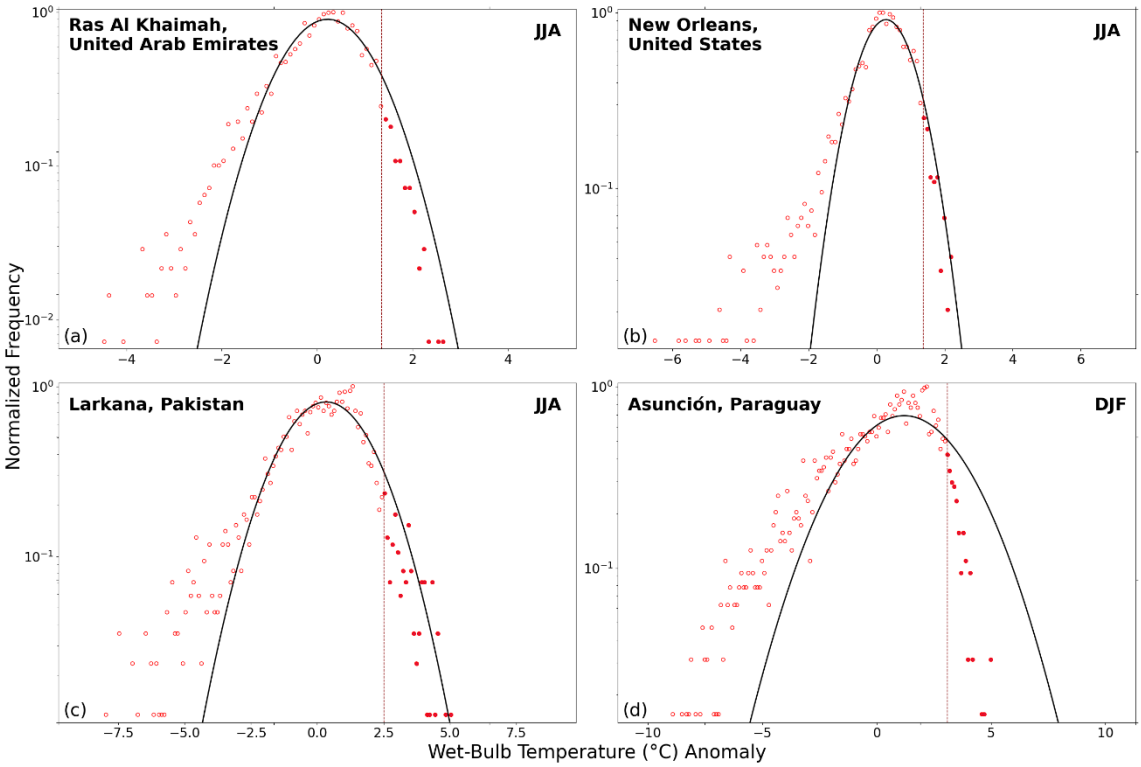

Figure 4. MERRA-2 PDFs of 1985-2014 T_W anomalies with a Gaussian curve fit to the core, plotted on a log-scale. In each subplot, the vertical dashed line indicates the historical 95th percentile, and points are histogram bin centers. Solid points represent the warm tail. Panel (a) is Ras Al Khaimah in the United Arab Emirates on the Persian Gulf coast in JJA, panel (b) is New Orleans, Louisiana in the United States in JJA, panel (c) is Larkana, Pakistan in JJA, and panel (d) is Asunción, Paraguay, in DJF.

5. Discussion

Since the identification of a theoretical physiological upper limit of T_W (Sherwood and Huber, 2010), much attention has been paid to the potential for humid-heat extremes to intensify under global warming (Matthews, 2018; Pal and Eltahir, 2016, Raymond et al., 2020; Schär, 2016). Studies that utilize climate models to analyze future T_W extremes often focus on global warming far above 2°C, such as 4°C (Schär, 2016), or even 7°C (Sherwood and Huber, 2010), or during the 30-year period of 2071-2100 when some CMIP6 models simulate a similarly high amount of warming under high-end emissions scenarios (Coffel et al., 2017; Pal and Eltahir, 2016). There are also several studies which examine the effect of warming on T_W at different emissions levels (Chen et al., 2022) and others which assess T_W under 1.5°C, 2°C warming, and 3°C (Freychet et al., 2022; Saeed et al., 2021; Wang et al., 2022). While these studies have in common an emphasis on the adaptability threshold of 35°C, instead we emphasize areas that may be regularly exposed to T_Ws which are classified as extreme in the recent climatology. This signal is sufficiently captured with 2°C warming, which is likely to occur without considerable near-term global mobilization around decarbonization. Furthermore, recent research implies that the human adaptability limit may actually be around 31°C, and probably lower in older people or those with certain underlying health conditions (Vecellio et al., 2022), though more research is needed. T_Ws of 31°C and above are very uncommon today, but not as rare as 35°C. An over-emphasis on the 35°C T_W threshold may overlook locations which are at high-risk of dangerous moist-heat stress in the near future. Nevertheless, the adaptability threshold is still an important consideration, especially because several degrees of global warming is possible without climate change mitigation.

The non-Gaussian nature of temperature has been previously used to identify regions at risk of extreme heat under global warming (Loikith et al., 2018; Loikith and Neelin, 2015; Loikith and Neelin, 2019; Ruff and Neelin, 2012*).* Analysis of tail shape is not as useful in locations with low variance. When σ is less than 1°C T_W, the PDF is shifted so far to the right of the original PDF that tail shape is practically inconsequential. Some analyses of increases in humid-heat extremes assume Gaussianity of the underlying PDFs at each location, identifying significant shifts up to 3σ in the time period of 2000-2012 in the tropics (Coumou and Robinson, 2013). We find that this similarly applies to T_W when σ is less than about 1°C, no matter the shape of the underlying PDF, since even a modest warming shifts the core of the distribution to the right of the pre-shifted 95th percentile. When assessed globally and especially outside the tropics, T_W distribution tail shape is well-correlated with future extreme threshold exceedances. This is in accordance with prior research on temperature distribution tails and extreme exceedances (Loikith et al., 2018; Loikith and Neelin, 2015; Loikith and Neelin, 2019).

It is theorized that the atmospheric dynamics from approximately 20°S to 20°N limit T_W warming to 1°C per 1°C tropical mean warming, possibly preventing extremes from reaching the 35°C threshold (Zhang et al., 2021). Although the theoretical adaptability limit may not be reached, a daily mean T_W which is almost always above 26°C in the summer months would create substantial public health and infrastructure challenges, despite possibly never breaching the adaptability threshold, such as in Cancún, Mexico and Darwin, Australia, as represented by our analysis (see Appendix Figure A6). Cancún has relatively low variability of its T_W PDF, and under a 2°C rise in global average temperature may observe daily mean temperatures in JJA which hinder all

outdoor activities. In addition, our analysis utilizes a daily mean instead of a maximum T_W, so a breach of the adaptability threshold cannot be ruled out. The low spatiotemporal resolution of our data also undoubtedly underestimates extremes, as both low extremes and more moderate values are averaged with hot extremes. Such high daily mean T_W can be suggestive of high nighttime T_W, a time when humans are especially vulnerable to heat stress (Kravchenko et al., 2013). It is possible that in some cases, the prevailing meteorology that causes the short-tails may also prevent T_W from becoming too high, similar to the possible ceiling for T_W due to atmospheric constraints in the tropics (Sherwood and Huber, 2010; Zhang et al., 2021).

Although the relationships between humidity and temperature are well-understood (Fischer and Knutti, 2013), the relative contributions of humidity and heat to the risk of human heat stress still needs further investigation (Lutsko, 2021). Prior research suggests that latitude, topography (Raymond et al., 2022), or other geographic and climatological factors (Buzan et al., 2015; Ivanovich et al., 2022; Raymond et al., 2017; Wang et al., 2019; Zhao et al., 2015) can all be influential. This analysis suggests that, in general and on the global scale, specific humidity is more closely correlated to T_W extreme exceedances than temperature. This agrees with what Lutsko found with equivalent temperature in 2021, Coffel et al. found with T_W in 2019, and Raymond et al. found with T_W in 2017. Buzan and Huber found that T_W generally aligned with extreme temperature, but Heat Index and simple wet-bulb globe temperature aligned with temperature (2020). Our analysis also supports that humidity and heat combined provide a more robust assessment of T_W extremes, in agreement with Fischer and Knutti (2013). Experimental research which has examined the human body's response to different levels of heat and

humidity is sparse, but a recent study suggests that hotter, dryer T_W extremes may stress the body more than warm, humid, T_W extremes (Vecellio, et al., 2022). Utilizing controlled conditions indoors, this experiment found that body temperature rose in hotter, drier conditions of equal T_W to very humid, but less hot environments. If the human body responds differently to T_Ws that are of higher temperature and relatively lower humidity, then a possible next step would be to ascertain the different types of T_W extremes, for example, high temperature and lower humidity or lower temperature and higher humidity.

Long-tails may assist in the identification of areas which are at risk of very large excursions from the mean, such as was witnessed in the June 2021 heatwave in the Pacific Northwest of the United States which was outside the temperature distribution of the area in which it occurred (Thompson et al., 2022). This area has a long-tail of its temperature distribution (Loikith et al., 2018), so it can be expected that its local temperature extremes might fall past the hot end of the distribution during an event amplified by global warming. Long-tailed areas may be especially unprepared for extreme heat events. A similar case can be made for T_W and its long-tailed distributions. While certain short-tailed locations might endure persistently dangerous T_Ws during the warm season, it is also possible that long-tailed locations might experience T_Ws that the local populace may be completely unprepared for. These locations may also be the most at-risk of breaching the human adaptability threshold of 35°C T_W. Even though our analysis focuses on short-tails, the implications of long-tails are also relevant.

There are some limitations to this study. Certain regions which are at high-risk of dangerous T_W observe their highest temperatures outside of the summer months, such as

May in the northern hemisphere. Additionally, it is possible that in some locations higher spring temperatures mimic summer conditions. In certain climates, high temperatures may interact with terrestrial moisture sources to induce higher T_{WS}s (Freychet et al., 2020; Im et al., 2017). Changes in distribution shape may also not be effectively captured by the models, even though distribution shape is overall sufficient in the historical simulation when compared with reanalysis data. Unpredictable changes in human society or in the global climate cannot be accounted for in climate models. CMIP6 may also not accurately identify the 30-year time period in which there is a 2°C rise in global average temperatures, so the timeline for predicted adaptation may be difficult to determine. Despite these limitations, this study supports that our methodology is effective in identifying regions at increased risk of high T_W.

6. Conclusions

This research demonstrates that T_W distribution tail shape has a significant effect on future extreme threshold exceedances under 2°C global warming as simulated by CMIP6 models. Short-tails on the warm-side of the T_W distribution are of particular concern as they may indicate a very large number of future exceedances over the current-climate 95th percentile. Although this analysis suggests that long-tails result in a slower increase in extreme exceedances in comparison to Gaussian- or shorter-tails, long-tails can still be impactful in areas which are unprepared for extreme T_W due to its relative rarity. We also find that specific humidity has a larger contribution to projected T_W extremes than temperature when assessed using our shift ratio methodology. The physical mechanisms behind this are outside the scope of this thesis, but a more thorough understanding of how specific humidity and temperature interact to produce T_W extremes may benefit the accurate projection of their future occurrence. Insight into the changing probability of extreme T_W and identifying locations at risk of T_Ws that dangerously challenge the human thermoregulatory system is essential in the adequate preparation for the human health and societal consequences of extreme humid-heat under global warming.

7. References

Alexander, L. V., Zhang, X., Peterson, T. C., Caesar, J., Gleason, B., Tank, A. M. G. K., et al. (2006). Global observed changes in daily climate extremes of temperature and precipitation. *Journal of Geophysical Research: Atmospheres*, *111*(D5). https://doi.org/10.1029/2005JD006290

Barnston, A. G., Lyon, B., Coffel, E. D., & Horton, R. M. (2020). Daily Autocorrelation and Mean Temperature/Moisture Rise as Determining Factors for Future Heat-Wave Patterns in the United States. *Journal of Applied Meteorology and Climatology*, *59*(10), 1735–1754. https://doi.org/10.1175/JAMC-D-19-0291.1

Barriopedro, D., Fischer, E. M., Luterbacher, J., Trigo, R. M., & García-Herrera, R. (2011). The Hot Summer of 2010: Redrawing the Temperature Record Map of Europe. *Science*. https://doi.org/10.1126/science.1201224

Berg, A., Lintner, B. R., Findell, K. L., Malyshev, S., Loikith, P. C., & Gentine, P. (2014). Impact of Soil Moisture–Atmosphere Interactions on Surface Temperature Distribution. *Journal of Climate*, *27*(21), 7976–7993. https://doi.org/10.1175/JCLI-D-13-00591.1

Buzan, J. R., & Huber, M. (2020). Moist Heat Stress on a Hotter Earth. *Annual Review of Earth and Planetary Sciences*, *48*(1), 623–655. https://doi.org/10.1146/annurev-earth-053018-060100

Buzan, J. R., Oleson, K., & Huber, M. (2015). Implementation and comparison of a suite of heat stress metrics within the Community Land Model version 4.5. *Geoscientific Model Development*, *8*(2), 151–170. https://doi.org/10.5194/gmd-8-151-2015

Chen, H., He, W., Sun, J., & Chen, L. (2022). Increases of extreme heat-humidity days endanger future populations living in China. *Environmental Research Letters*, *17*(6), 064013. https://doi.org/10.1088/1748-9326/ac69fc

Coffel, E. D., Horton, R. M., & Sherbinin, A. de. (2017). Temperature and humidity based projections of a rapid rise in global heat stress exposure during the 21st century. Environmental Research Letters, 13(1), 014001. https://doi.org/10.1088/1748-9326/aaa00e

Coffel, E. D., Horton, R. M., Winter, J. M., & Mankin, J. S. (2019). Nonlinear increases in extreme temperatures paradoxically dampen increases in extreme humid-heat. *Environmental Research Letters*, *14*(8), 084003. https://doi.org/10.1088/1748-9326/ab28b7

Coumou, D., & Robinson, A. (2013). Historic and future increase in the global land area affected by monthly heat extremes. *Environmental Research Letters*, *8*(3), 034018. https://doi.org/10.1088/1748-9326/8/3/034018

Davies-Jones, R. (2008). An Efficient and Accurate Method for Computing the Wet-Bulb Temperature along Pseudoadiabats. *Monthly Weather Review*, *136*(7), 2764–2785. https://doi.org/10.1175/2007MWR2224.1

Davis, R. E., McGregor, G. R., & Enfield, K. B. (2016). Humidity: A review and primer on atmospheric moisture and human health. *Environmental Research*, *144*, 106–116. https://doi.org/10.1016/j.envres.2015.10.014

de Freitas, C. R., & Grigorieva, E. A. (2015). A comprehensive catalogue and classification of human thermal climate indices. *International Journal of Biometeorology*, *59*(1), 109–120. https://doi.org/10.1007/s00484-014-0819-3

Dosio, A., Mentaschi, L., Fischer, E. M., & Wyser, K. (2018). Extreme heat waves under 1.5\hspace0.167em°C and 2\hspace0.167em°C global warming. Environmental Research Letters, 13(5), 054006. https://doi.org/10.1088/1748-9326/aab827

Dunne, J. P., Stouffer, R. J., & John, J. G. (2013). Reductions in labour capacity from heat stress under climate warming. *Nature Climate Change*, *3*(6), 563–566. https://doi.org/10.1038/nclimate1827

Eyring, V., Bony, S., Meehl, G. A., Senior, C. A., Stevens, B., Stouffer, R. J., & Taylor, K. E. (2016). Overview of the Coupled Model Intercomparison Project Phase 6 (CMIP6) experimental design and organization. *Geoscientific Model Development*, *9*(5), 1937–1958. https://doi.org/10.5194/gmd-9-1937-2016

Fischer, E. M., & Knutti, R. (2013). Robust projections of combined humidity and temperature extremes. *Nature Climate Change*, *3*(2), 126–130. https://doi.org/10.1038/nclimate1682

Friedrich, T., Timmermann, A., Tigchelaar, M., Elison Timm, O., & Ganopolski, A. (2016). Nonlinear climate sensitivity and its implications for future greenhouse warming. *Science Advances*, *2*(11), e1501923. https://doi.org/10.1126/sciadv.1501923

Freychet, N., Hegerl, G. C., Lord, N. S., Lo, Y. T. E., Mitchell, D., & Collins, M. (2022). Robust increase in population exposure to heat stress with increasing global warming. *Environmental Research Letters*, *17*(6), 064049. https://doi.org/10.1088/1748-9326/ac71b9

Freychet, N., Tett, S. f. b., Yan, Z., & Li, Z. (2020). Underestimated Change of Wet-Bulb Temperatures Over East and South China. *Geophysical Research Letters*, *47*(3), e2019GL086140. https://doi.org/10.1029/2019GL086140

Garfinkel, C. I., & Harnik, N. (2017). The Non-Gaussianity and Spatial Asymmetry of Temperature Extremes Relative to the Storm Track: The Role of Horizontal Advection. *Journal of Climate*, *30*(2), 445–464. https://doi.org/10.1175/JCLI-D-15-0806.1

Gelaro, R., McCarty, W., Suárez, M. J., Todling, R., Molod, A., Takacs, L., et al. (2017). The Modern-Era Retrospective Analysis for Research and Applications, Version 2 (MERRA-2). *Journal of Climate*, *30*(14), 5419–5454. https://doi.org/10.1175/JCLI-D-16-0758.1

Held, I. M., & Soden, B. J. (2000). Water Vapor Feedback and Global Warming. Annual Review of Energy and the Environment, 25(1), 441–475. https://doi.org/10.1146/annurev.energy.25.1.441

Haldane, J. S. (1905). The Influence of High Air Temperatures No. I. *Epidemiology & Infection*, *5*(4), 494–513. https://doi.org/10.1017/S0022172400006811

Im, E.-S., Pal, J. S., & Eltahir, E. A. B. (2017). Deadly heat waves projected in the densely populated agricultural regions of South Asia. Science Advances, 3(8), e1603322. https://doi.org/10.1126/sciadv.1603322

IPCC, 2021: Climate Change 2021: The Physical Science Basis. Contribution of Working Group I to the Sixth Assessment Report of the Intergovernmental Panel on Climate Change [Masson-Delmotte, V., P. Zhai, A. Pirani, S.L. Connors, C. Péan, S. Berger, N. Caud, Y. Chen, L. Goldfarb, M.I. Gomis, M. Huang, K. Leitzell, E. Lonnoy, J.B.R. Matthews, T.K. Maycock, T. Waterfield, O. Yelekçi, R. Yu, and B. Zhou (eds.)]. Cambridge University Press, Cambridge, United Kingdom and New York, NY, USA, In press, https://doi:10.1017/9781009157896

Ivanovich, C., Anderson, W., Horton, R., Raymond, C., & Sobel, A. (2022). The Influence of Intraseasonal Oscillations on Humid Heat in the Persian Gulf and South Asia. *Journal of Climate*, *35*(13), 4309–4329. https://doi.org/10.1175/JCLI-D-21-0488.1

Kopp, B. (2016). WetBulb.m. Retrieved from https://github.com/bobkopp/WetBulb.m

Kravchenko, J., Abernethy, A. P., Fawzy, M., & Lyerly, H. K. (2013). Minimization of Heatwave Morbidity and Mortality. *American Journal of Preventive Medicine*, *44*(3), 274–282. https://doi.org/10.1016/j.amepre.2012.11.015

Li, Xianxiang. (2019). WetBulb.py. Retrieved from https://github.com/smartlixx/WetBulb

Linz, M., Chen, G., & Hu, Z. (2018). Large-Scale Atmospheric Control on Non-Gaussian Tails of Midlatitude Temperature Distributions. *Geophysical Research Letters*, *45*(17), 9141–9149. https://doi.org/10.1029/2018GL079324

Loikith, P. C., & Neelin, J. D. (2015). Short-tailed temperature distributions over North America and implications for future changes in extremes. *Geophysical Research Letters*, *42*(20), 8577–8585. https://doi.org/10.1002/2015GL065602

Loikith, P. C., Neelin, J. D., Meyerson, J., & Hunter, J. S. (2018). Short Warm-Side Temperature Distribution Tails Drive Hot Spots of Warm Temperature Extreme Increases under Near-Future Warming. *Journal of Climate*, *31*(23), 9469–9487. https://doi.org/10.1175/JCLI-D-17-0878.1

Loikith, P. C., & Neelin, J. D. (2019). Non-Gaussian Cold-Side Temperature Distribution Tails and Associated Synoptic Meteorology. *Journal of Climate*, *32*(23), 8399–8414. https://doi.org/10.1175/JCLI-D-19-0344.1

Lutsko, N. J. (2021). The Relative Contributions of Temperature and Moisture to Heat Stress Changes under Warming. *Journal of Climate*, *34*(3), 901–917. https://doi.org/10.1175/JCLI-D-20-0262.1

Macpherson, R. K. (1962). The Assessment of the Thermal Environment. A Review. *Occupational and Environmental Medicine*, *19*(3), 151–164. https://doi.org/10.1136/oem.19.3.151

Matthews, T. (2018). Humid heat and climate change. *Progress in Physical Geography: Earth and Environment*, *42*(3), 391–405. https://doi.org/10.1177/0309133318776490

Miralles, D. G., Teuling, A. J., van Heerwaarden, C. C., & Vilà-Guerau de Arellano, J. (2014). Mega-heatwave temperatures due to combined soil desiccation and atmospheric heat accumulation. *Nature Geoscience*, *7*(5), 345–349. https://doi.org/10.1038/ngeo2141

Mora, C., Dousset, B., Caldwell, I. R., Powell, F. E., Geronimo, R. C., Bielecki, C. R., et al. (2017). Global risk of deadly heat. *Nature Climate Change*, *7*(7), 501–506. https://doi.org/10.1038/nclimate3322

Pal, J. S., & Eltahir, E. A. B. (2016). Future temperature in southwest Asia projected to exceed a threshold for human adaptability. *Nature Climate Change*, *6*(2), 197–200. https://doi.org/10.1038/nclimate2833

Perkins, S. E., Alexander, L. V., & Nairn, J. R. (2012). Increasing frequency, intensity and duration of observed global heatwaves and warm spells. *Geophysical Research Letters*, *39*(20). https://doi.org/10.1029/2012GL053361

Perron, M., & Sura, P. (2013). Climatology of Non-Gaussian Atmospheric Statistics. *Journal of Climate*, *26*(3), 1063–1083. https://doi.org/10.1175/JCLI-D-11-00504.1

Rastogi, D., Lehner, F., & Ashfaq, M. (2020). Revisiting Recent U.S. Heat Waves in a Warmer and More Humid Climate. *Geophysical Research Letters*, *47*(9), e2019GL086736. https://doi.org/10.1029/2019GL086736

Raymond, C., Matthews, T., & Horton, R. M. (2020). The emergence of heat and humidity too severe for human tolerance. *Science Advances*, *6*(19), eaaw1838. https://doi.org/10.1126/sciadv.aaw1838

Raymond, C., Singh, D., & Horton, R. M. (2017). Spatiotemporal Patterns and Synoptics of Extreme Wet-Bulb Temperature in the Contiguous United States. *Journal of Geophysical Research: Atmospheres*, *122*(24), 13,108-13,124. https://doi.org/10.1002/2017JD027140

Raymond, C., Waliser, D., Guan, B., Lee, H., Loikith, P., Massoud, E., et al. (2022). Regional and elevational patterns of extreme heat stress change in the US. *Environmental Research Letters*, *17*(6), 064046. https://doi.org/10.1088/1748-9326/ac7343

Robine, J.-M., Cheung, S. L. K., Le Roy, S., Van Oyen, H., Griffiths, C., Michel, J.-P., & Herrmann, F. R. (2008). Death toll exceeded 70,000 in Europe during the summer of 2003. Comptes Rendus Biologies, 331(2), 171–178. https://doi.org/10.1016/j.crvi.2007.12.001

Ruff, T. W., & Neelin, J. D. (2012). Long-tails in regional surface temperature probability distributions with implications for extremes under global warming. *Geophysical Research Letters*, *39*(4). https://doi.org/10.1029/2011GL050610

Russo, S., Sillmann, J., & Sterl, A. (2017). Humid heat waves at different warming levels. *Scientific Reports*, *7*(1), 7477. https://doi.org/10.1038/s41598-017-07536-7

Saeed, F., Schleussner, C.-F., & Ashfaq, M. (2021). Deadly Heat Stress to Become Commonplace Across South Asia Already at 1.5°C of Global Warming. *Geophysical Research Letters*, *48*(7), e2020GL091191. https://doi.org/10.1029/2020GL091191

Santer, B. D., Mears, C., Wentz, F. J., Taylor, K. E., Gleckler, P. J., Wigley, T. M. L., et al. (2007). Identification of human-induced changes in atmospheric moisture content. Proceedings of the National Academy of Sciences, 104(39), 15248–15253. https://doi.org/10.1073/pnas.0702872104

Schär, C. (2016). The worst heat waves to come. *Nature Climate Change*, *6*(2), 128–129. https://doi.org/10.1038/nclimate2864

Seneviratne, S. I., Corti, T., Davin, E. L., Hirschi, M., Jaeger, E. B., Lehner, I., et al. (2010). Investigating soil moisture–climate interactions in a changing climate: A review. *Earth-Science Reviews*, *99*(3), 125–161. https://doi.org/10.1016/j.earscirev.2010.02.004

Seneviratne, S. I., Donat, M. G., Pitman, A. J., Knutti, R., & Wilby, R. L. (2016). Allowable CO2 emissions based on regional and impact-related climate targets. *Nature*, *529*(7587), 477–483. https://doi.org/10.1038/nature16542

Sherwood, S. C., & Huber, M. (2010). An adaptability limit to climate change due to heat stress. *Proceedings of the National Academy of Sciences*, *107*(21), 9552–9555. https://doi.org/10.1073/pnas.0913352107

Skinner, C. B., Poulsen, C. J., & Mankin, J. S. (2018). Amplification of heat extremes by plant CO2 physiological forcing. *Nature Communications*, *9*(1), 1094. https://doi.org/10.1038/s41467-018-03472-w

Steadman, R. G. (1979). The Assessment of Sultriness. Part I: A Temperature-Humidity Index Based on Human Physiology and Clothing Science. *Journal of Applied Meteorology and Climatology*, *18*(7), 861–873. https://doi.org/10.1175/1520-0450(1979)018<0861:TAOSPI>2.0.CO;2

Thompson, V., Kennedy-Asser, A. T., Vosper, E., Lo, Y. T. E., Huntingford, C., Andrews, O., et al. (2022). The 2021 western North America heat wave among the most extreme events ever recorded globally. *Science Advances*, *8*(18), eabm6860. https://doi.org/10.1126/sciadv.abm6860

van Oldenborgh, G. J., Philip, S., Kew, S., van Weele, M., Uhe, P., Otto, F., et al. (2018). Extreme heat in India and anthropogenic climate change. *Natural Hazards and Earth System Sciences*, *18*(1), 365–381. https://doi.org/10.5194/nhess-18-365-2018

Vanos, J. K., Baldwin, J. W., Jay, O., & Ebi, K. L. (2020). Simplicity lacks robustness when projecting heat-health outcomes in a changing climate. *Nature Communications*, *11*(1), 6079. https://doi.org/10.1038/s41467-020-19994-1

Vecellio, D. J., Wolf, S. T., Cottle, R. M., & Kenney, W. L. (2022). Evaluating the 35°C wet-bulb temperature adaptability threshold for young, healthy subjects (PSU HEAT Project). *Journal of Applied Physiology*, *132*(2), 340–345. https://doi.org/10.1152/japplphysiol.00738.2021

Wang, X.-S., He, L., Ma, X.-H., Bie, Q., Luo, L., Xiong, Y.-C., & Ye, J.-S. (2022). The emergence of prolonged deadly humid heatwaves. *International Journal of Climatology*, *n/a*(n/a). https://doi.org/10.1002/joc.7750

Wang, P., Leung, L. R., Lu, J., Song, F., & Tang, J. (2019). Extreme Wet-Bulb Temperatures in China: The Significant Role of Moisture. *Journal of Geophysical Research: Atmospheres*, *124*(22), 11944–11960. https://doi.org/10.1029/2019JD031477

Wehner, M., Stone, D., Krishnan, H., AchutaRao, K., & Castillo, F. (2016). 16. THE DEADLY COMBINATION OF HEAT AND HUMIDITY IN INDIA AND PAKISTAN IN SUMMER 2015. Bulletin of the American Meteorological Society, 97(12), S81–S86. https://doi.org/10.1175/BAMS-D-16-0145.1

Wheeler, P. E. (1991). The thermoregulatory advantages of hominid bipedalism in open equatorial environments: the contribution of increased convective heat loss and cutaneous evaporative cooling. *Journal of Human Evolution*, *21*(2), 107–115. https://doi.org/10.1016/0047-2484(91)90002-D

Willett, K. M., Gillett, N. P., Jones, P. D., & Thorne, P. W. (2007). Attribution of observed surface humidity changes to human influence. Nature, 449(7163), 710–712. https://doi.org/10.1038/nature06207

Willett, K. M., & Sherwood, S. (2012). Exceedance of heat index thresholds for 15 regions under a warming climate using the wet-bulb globe temperature. International Journal of Climatology, 32(2), 161–177. https://doi.org/10.1002/joc.2257

Yaglou, C. P., & Minaed, D. (1957). Control of Heat Casualties at Military Training Centers. *Arch. Indust. Health*, *16*(4), 302–16. https://doi.org/10.1001/jama.1957.02980320043010

Zelinka, M. D., Myers, T. A., McCoy, D. T., Po-Chedley, S., Caldwell, P. M., Ceppi, P., et al. (2020). Causes of Higher Climate Sensitivity in CMIP6 Models. *Geophysical Research Letters*, *47*(1), e2019GL085782. https://doi.org/10.1029/2019GL085782

Zhang, Y., Held, I., & Fueglistaler, S. (2021). Projections of tropical heat stress constrained by atmospheric dynamics. *Nature Geoscience*, *14*(3), 133–137. https://doi.org/10.1038/s41561-021-00695-3

Zhao, Y., Ducharne, A., Sultan, B., Braconnot, P., & Vautard, R. (2015). Estimating heat stress from climate-based indicators: present-day biases and future spreads in the CMIP5 global climate model ensemble. *Environmental Research Letters*, *10*(8), 084013. https://doi.org/10.1088/1748-9326/10/8/084013

Appendix: Supplementary Figures and Tables

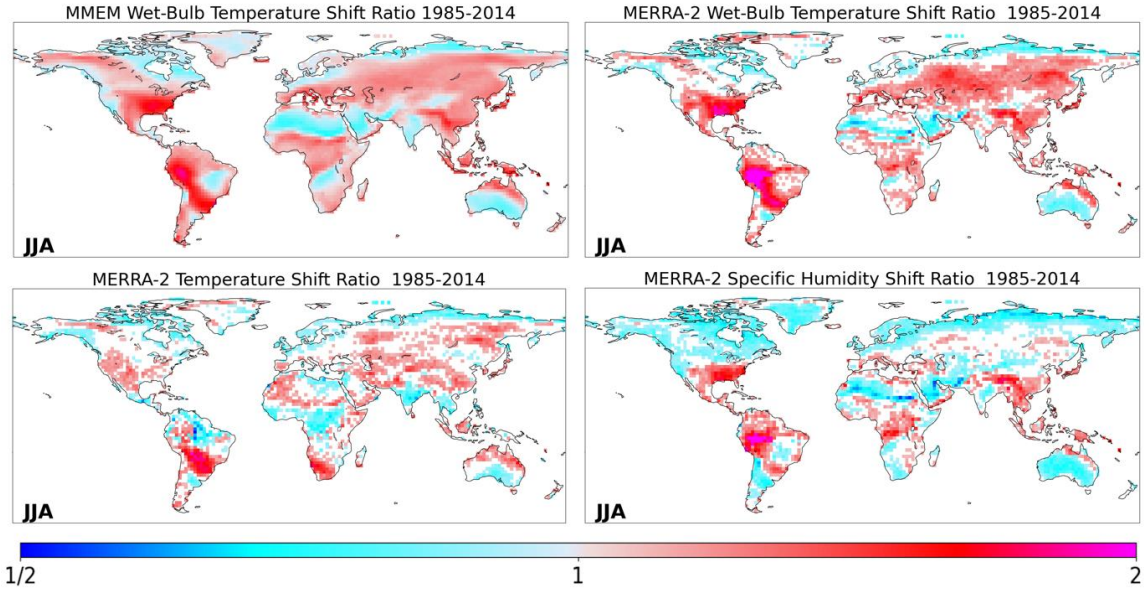

Figure A1. The multi-model ensemble mean shift ratio for T_W, the MERRA-2 T_W shift ratio, the MERRA-2 temperature shift ratio, and the MERRA-2 specific humidity shift ratio for JJA.

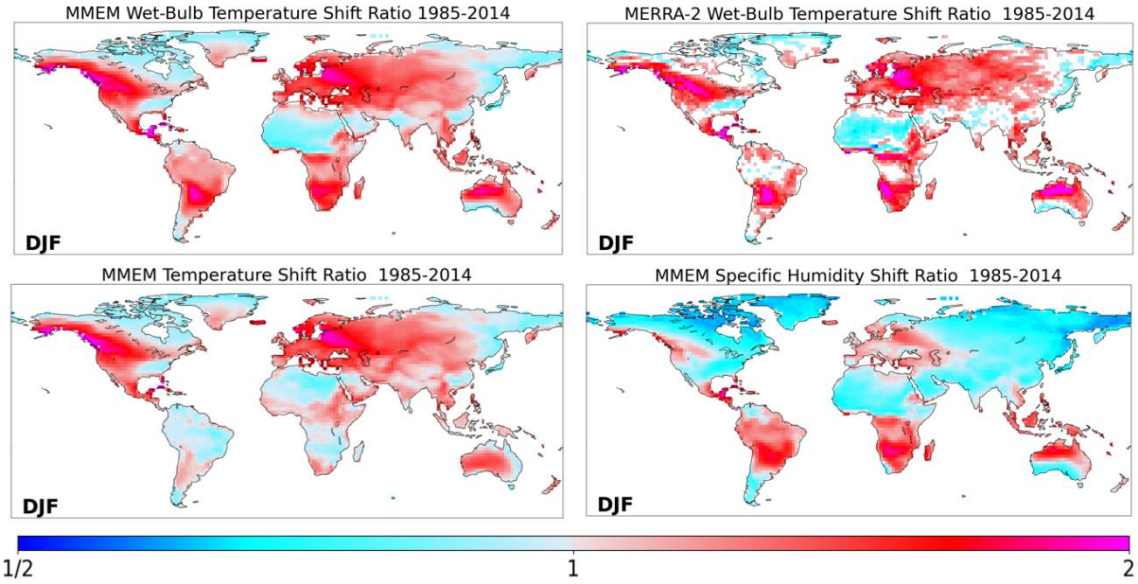

Figure A2. The multi-model ensemble mean shift ratio for T_W, the MERRA-2 T_W shift ratio, the MERRA-2 temperature shift ratio, and the MERRA-2 specific humidity shift ratio for JJA.

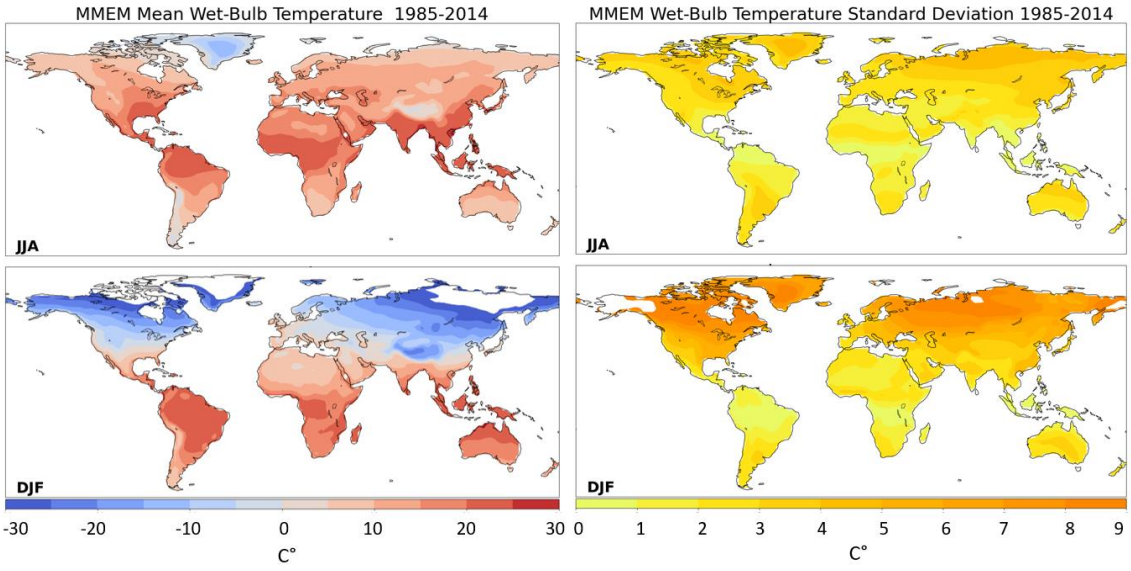

Figure A3. The MMEM mean T_W for JJA and DJF (left), and the MMEM standard deviation of T_W for JJA and DJF (right).

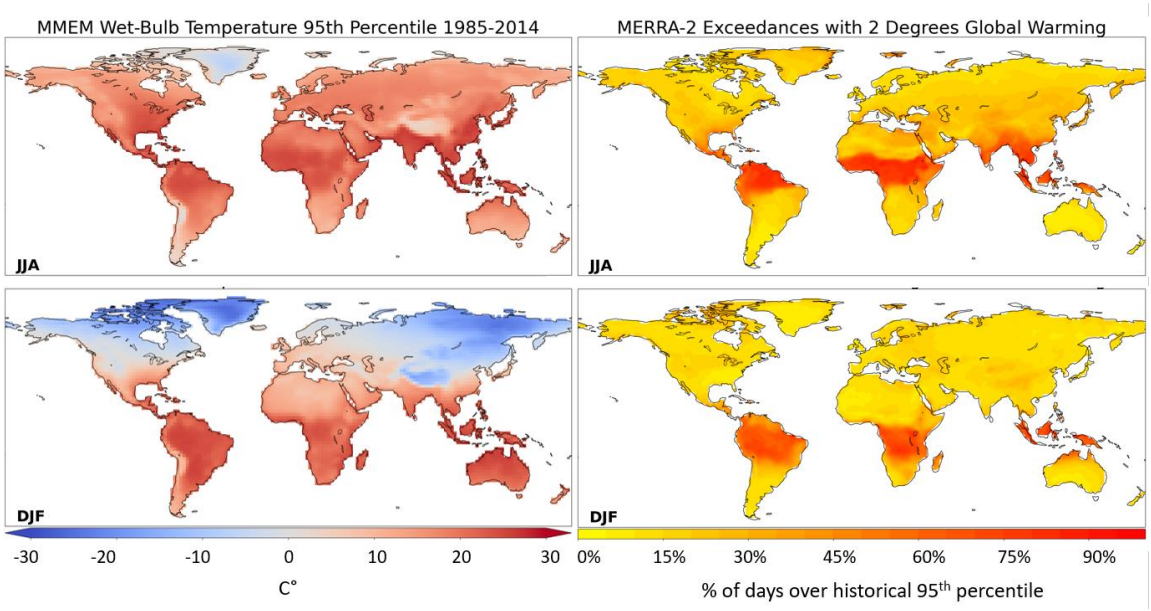

Figure A4. The MMEM 95th percentile of T_W for JJA and DJF (left), and the MERRA-2 exceedances with a rightward shift of the MMEM mean warming of T_W for JJA and DJF (right).

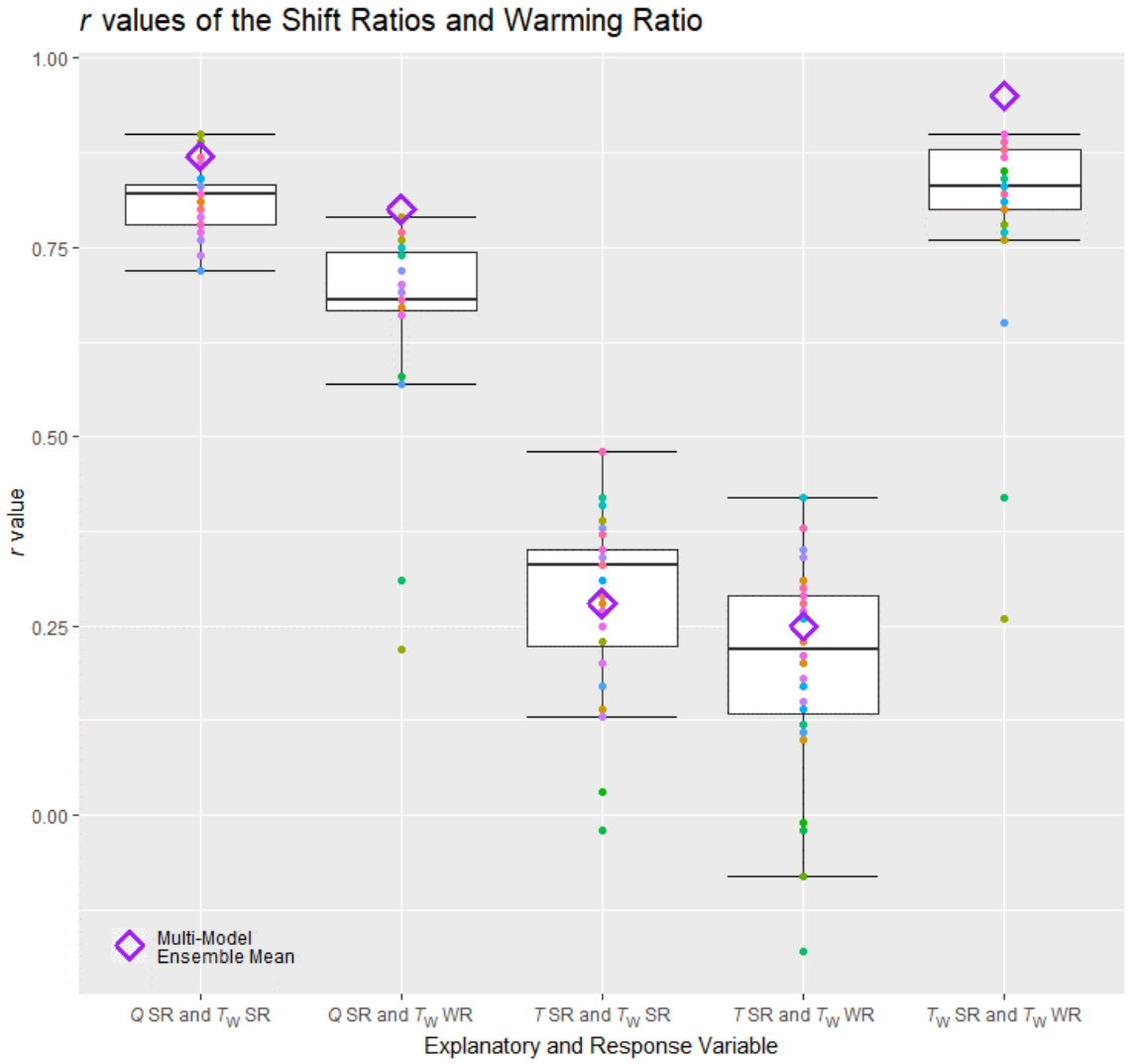

Figure A5. Box and whisker plot of *r* values for the T_W shift ratio (SR), air temperature (*T*) shift ratio, and specific humidity (*Q*) shift ratio, and the T_W warming ratio (WR) as in Table 2. Each point represents an individual CMIP6 model, and the purple diamond represents the MMEM.

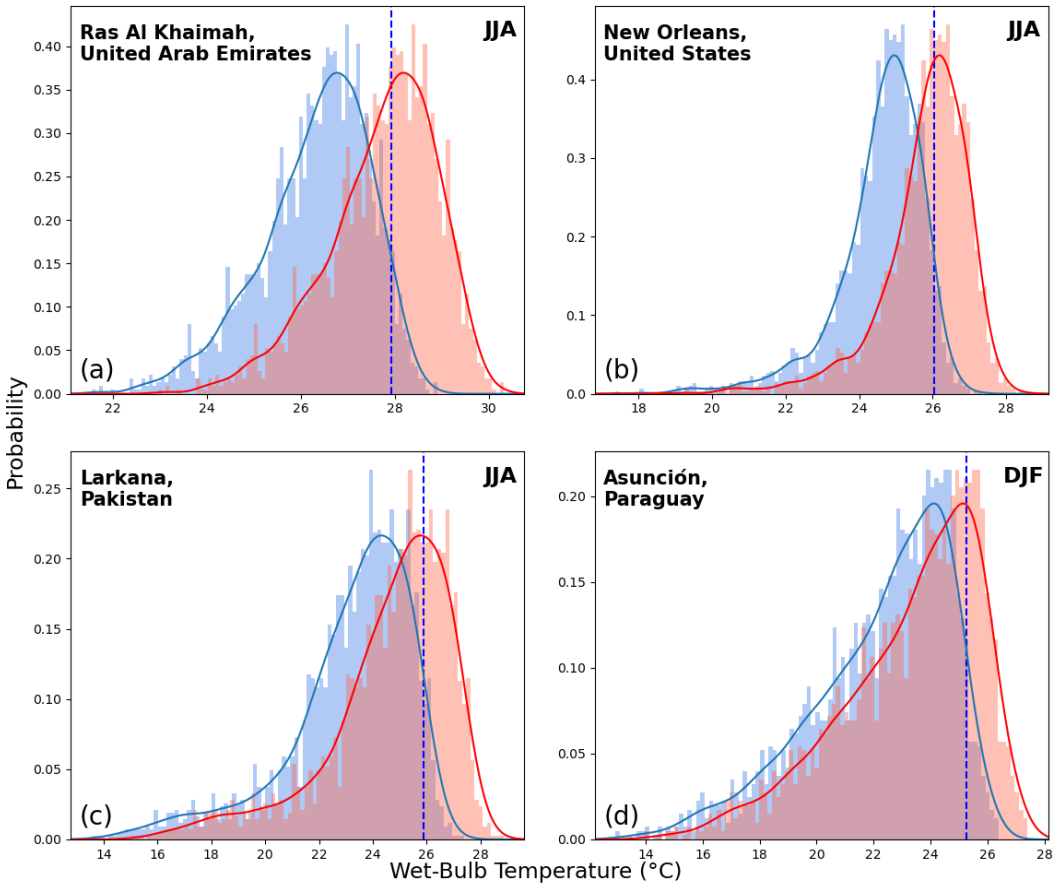

Figure A6. MERRA-2 wet-bulb temperature distributions of short-tailed locations shifted by the local $\Delta T_{\mathrm{W}}/\sigma_{\mathrm{historical}}$ with the MMEM of 2°Celsius global warming.

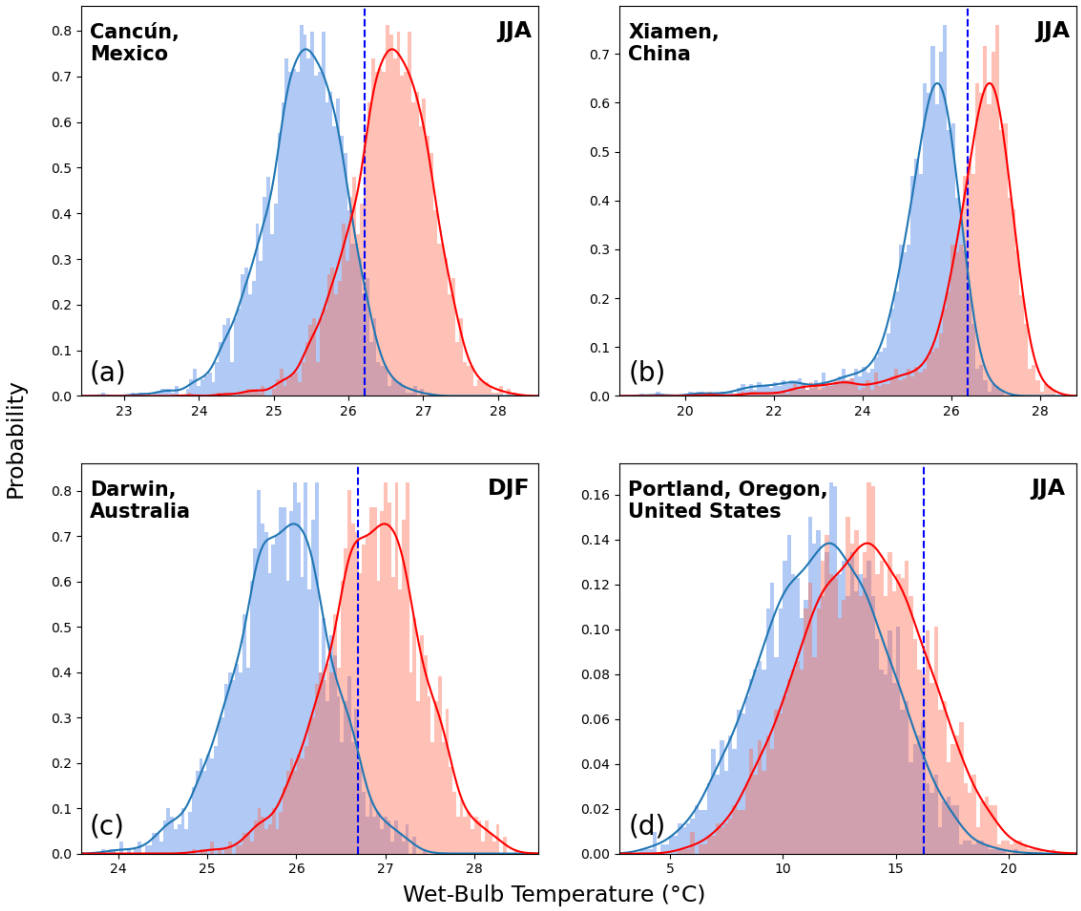

Figure A7. MERRA-2 wet-bulb temperature distributions shifted by the local $\Delta T_W/\sigma_{\text{historical}}$ with the MMEM of 2°Celsius global warming. (a-c) possess lower variance and (d) is a location with a Gaussian distribution.